

## Accepted Manuscript

Modelling the Synthesis of Nanoparticles in Continuous Microreactors: the Role of Diffusion and Residence Time Distribution on Nanoparticle Characteristics

Luca Panariello, Luca Mazzei, Asterios Gavriilidis

PII: S1385-8947(18)30525-4  
DOI: <https://doi.org/10.1016/j.cej.2018.03.167>  
Reference: CEJ 18774

To appear in: *Chemical Engineering Journal*

Received Date: 20 January 2018  
Revised Date: 21 March 2018  
Accepted Date: 29 March 2018



Please cite this article as: L. Panariello, L. Mazzei, A. Gavriilidis, Modelling the Synthesis of Nanoparticles in Continuous Microreactors: the Role of Diffusion and Residence Time Distribution on Nanoparticle Characteristics, *Chemical Engineering Journal* (2018), doi: <https://doi.org/10.1016/j.cej.2018.03.167>

This is a PDF file of an unedited manuscript that has been accepted for publication. As a service to our customers we are providing this early version of the manuscript. The manuscript will undergo copyediting, typesetting, and review of the resulting proof before it is published in its final form. Please note that during the production process errors may be discovered which could affect the content, and all legal disclaimers that apply to the journal pertain.

# Modelling the Synthesis of Nanoparticles in Continuous Microreactors: the Role of Diffusion and Residence Time Distribution on Nanoparticle Characteristics

*Luca Panariello, Luca Mazzei\*, Asterios Gavriilidis\**

*Department of Chemical Engineering, University College London, Torrington Place, London, WC1E 7JE*

*\*Corresponding authors: [l.mazzei@ucl.ac.uk](mailto:l.mazzei@ucl.ac.uk), [a.gavriilidis@ucl.ac.uk](mailto:a.gavriilidis@ucl.ac.uk)*

## Abstract

A mathematical model for the liquid-phase synthesis of spherical nanoparticles in continuous flow micro- and milli-reactors was developed, accounting for residence time distributions (RTD). These distributions were derived for the reactants and the particles involved in the synthesis. The kinetic parameters needed to describe the reactions were calculated from experimental data available in the literature from batch reactors, with the aid of population balance modelling. They were subsequently used, without further modification, to simulate the synthesis in flow reactors via population balance modelling, averaging the results at the reactor outlet using the reactor RTDs. The model was employed to describe the synthesis of silica nanoparticles as a case study, and validated against flow reactor results from the literature. The results demonstrate direct RTD effects and indirect diffusion-induced effects on the evolution of the particle size distribution during the flow synthesis. The former are created by the inherent widening of the RTDs, due to the different residence time experienced by each fluid element, leading to a broadening of the particle size distribution. The latter are induced by the difference in diffusivity between nanoparticles and liquid reactants, which leads to different dispersion processes in the reactor for the different components of the reaction mixture. These effects appear as the major cause of particle size distribution difference between (single phase) flow and batch syntheses.

## 1. Introduction

Nanomaterials are a research topic of interest in many areas, such as electronics, energy, biotechnology, medicine, bio-imaging, gene and drug delivery [1–8]. Currently, these materials are synthesized mostly in batch mode; however, in these procedures the size distribution of the particles and the quality of the product between batches are often irreproducible. Furthermore, fast screening procedures are difficult to implement in batch operations, and difficulties in scaling up these systems are encountered (e.g. achieving homogeneous concentration and temperature conditions in batch reactors at the timescales required can be challenging).

Nanomaterials synthesis in continuous-flow systems is nowadays gaining increasing interest. Continuous reactors allow high productivity as well as enhanced controllability of the processes and easy implementation of on-line quality control devices [9]. Milli- and microreactors represent a useful tool to achieve consistent continuous nanoparticle production by liquid phase syntheses. Furthermore, the use of small channel reactors can lead to process intensification [10,11], allowing a marked reduction in size of chemical plants, with an increase in their efficiency, due to improved mass and heat transfer, as well as enabling safer and more sustainable processes.

One of the challenges that must be tackled to adopt these processes for real industrial applications is scalability. An efficient scale-up procedure requires the understanding of the spatio-temporal evolution of the reactions and transport phenomena involved in the process. In this way, more refined design procedures can be developed, overcoming a purely *black-box* approach. The number and complexity of nanostructures that it is possible to synthesize without a deep understanding of the physical and chemical aspects involved in their synthesis processes is nevertheless impressive; the situation is well described by Xia et al. [12] who report that “at the current stage of development, it is not an exaggeration to say that the chemical synthesis of metal nanocrystals (as well as for other solid materials) remains an art rather than a

science". In recent years an increasing interest in the modeling of these syntheses has appeared, generally based on the use of population balance modelling [13–16].

The present study aims to highlight some of the phenomena that lead to differences between flow and batch processes, and to propose a method for the design of flow reactors that allows the prediction of their output in terms of the particle size distribution. Starting from a classic reactor engineering approach [17], relevant dimensionless numbers have been evaluated to derive a set of equations able to describe milli- and microreactors characterized by common flow patterns and employed for the synthesis of spherical nanoparticles. Due to their dimensions, milli- and microreactors are characterized by low values of the Reynolds number [18], and so the flow regime is laminar. In particular two configurations have been analyzed: straight tube single-phase Laminar Flow Reactors (LFR) and two-phase Segmented Flow Reactors (SFR). The model proposed is employed to describe the synthesis of silica nanoparticles through the Stöber process, used as a case study. The choice of the Stöber process, a well-established and deeply understood and characterized colloidal synthesis, allowed us to focus on the relevant transport phenomena occurring in the reactors, which is the main objective of this work. The results of the model are eventually validated against data taken from the literature.

This paper is organized as follows: in Section 2 the RTDs for the different species involved in the synthesis are analyzed for the two reactors mentioned (LFR and SFR). In Section 3, the kinetic parameters needed to describe the flow synthesis are derived, with the aid of population balance modelling, from experimental data of batch reactors available in the literature. Starting from the framework described in these two sections, the problem of predicting the outcome of a continuous synthesis is tackled in Section 4, and the results of the model are therein discussed. Finally, in Section 5 the conclusions of the work are presented.

## 2. Residence time distribution in milli- and microreactors for spherical nanoparticles synthesis

Residence time distributions represent a useful tool in reactor design, especially when deviations from ideal flow patterns (such as plug flow) play a key role in determining the reactor performance [17]. These deviations are important in the continuous synthesis of nanomaterials, where differences between flow and batch processes, as well as between flow syntheses carried out under different flow regimes, have been reported [9,19–21], and attributed to RTD-effects in the reactors employed for the synthesis, where each fluid element experiences a residence time that is different from the average value.

This study aims to predict the performance of these reactors. In particular two classes of reactors commonly employed will be analyzed, namely single-phase Laminar Flow Reactors (LFRs) and two-phase Segmented Flow Reactors (SFRs). Compared to the latter, LFRs are easier to be implemented, do not require any auxiliary fluid to achieve the desired flow regime (fluid that needs to be separated from the product, introducing the necessity of a further separation unit at the outlet of the reactor) and, given the reactor volume, allows the use of higher flow rates for a given residence time. However, LFRs are generally characterized by wider particle size distributions (due to wider RTDs) and are affected more by fouling problems than the SFRs. Still, in the literature robust syntheses of nanoparticles in these devices are reported [9,19,21–23]. Hence, the description of both reactor classes is considered here.

In this section the RTD for the LFRs is first determined. Interestingly, in these reactors different RTDs characterize the different species involved in the synthesis (particles and liquid reactants). This is due to their marked different diffusivities, which lead to deviations from ideal flow patterns not only ascribable to the RTDs inherent width (that leads to the production of more dispersed particles compared to batch syntheses), but also to less intuitive and case-dependent effects that indirectly influence the chemistry of

the process, as it will be discussed in detail in Section 4.3. The RTD of SFRs is then derived and compared with that of LFRs.

## 2.1 Single-phase Laminar Flow Reactors

In single-phase reactors, the reaction mixture is simply pumped through an aging channel after a mixing section in which the reactants streams are well mixed. We will focus on systems characterized by low Dean number values, so that the reactor can be considered equivalent to a straight tube [24]. The RTD can then be estimated following the results of Ananthkrishnan and co-workers [17][25], which are presented in terms of two dimensionless quantities: the aspect ratio of the reactor  $L/d_t$ , where  $L$  is the length of the reactor and  $d_t$  is its diameter, and the Bodenstein number  $Bo = ud_t/D_m$ , where  $u$  is the fluid average superficial velocity and  $D_m$  is the reactant molecular diffusivity.

Ananthkrishnan and coworkers [25] found that the RTD of a single phase laminar flow reactor can be described by three different models, depending on the values of the  $Bo$  number and aspect ratio. Hence, three different regions are identified in the  $Bo - L/d_t$  plane, in which the following models need to be applied to describe the RTD:

- the pure convection model, where the RTD is related solely to the parabolic velocity profile of the fluid in the channel [17]. In this case, the convective transport in the axial direction dominates over the diffusive transport, both in the radial and axial directions;
- the Taylor-Aris model [26,27], or axial dispersion model, where radial diffusion is sufficiently strong to allow the molecules of a reactant to travel across the streamlines, so that their convective axial

transport can be described by means of the fluid average superficial velocity  $u$ . When this model is valid, in addition to the convective contribution, the axial mass transfer of the reactant includes a *diffusion-like* process superimposed to the plug flow. Referred to as *axial dispersion*, this process is described through an axial dispersion coefficient  $D_{ax}$ . According to this model, the (steady-state) mass balance equation for the reactant reads:

$$u \frac{dC}{dz} - D_{ax} \frac{d^2C}{dz^2} = r_{Gen} \quad (1)$$

where  $C$  is the reactant concentration,  $z$  is the axial coordinate and  $r_{Gen}$  is the reaction rate. Only when axial convection is dominant (that is, when  $D_{ax}/uL < 0.01$ ), this model reduces to the PFR (Plug Flow Reactor) model. The pure diffusion model, reported in the flow map from Ananthkrishnan et al. [25], is nothing but the Taylor-Aris model when it is possible to approximate  $D_{ax}$  with  $D_m$  [17];

- the transition region, in which neither of the two models described above is correct, because both convection and diffusion affect the RTD significantly.

For high values of the Dean number, this approach is no longer valid, and experimental or theoretical/numerical tests for the determination of the RTD are required [28].

RTD experiments for milli and microreactors indicate that in most applications the RTD of these reactors is described by the Taylor-Aris model [18,20,29]; this is because of the high values of the channel aspect ratio and the typically low superficial velocities. Since the  $Bo$  number depends on  $D_m$ , a key parameter in determining the correct RTD model is the molecular diffusivity. For liquids, the order of magnitude of  $D_m$  is  $10^{-9} \text{ m}^2/\text{s}$ , a value that renders the Taylor-Aris model applicable. However, the RTD has to be determined using a value of  $D_m$  that approximates that of the reactants. In case of the synthesis of nanoparticles, the reaction mixture is quite complex, since multiple reactants are involved, characterized by different diffusivities, which can vary by orders of magnitude; hence, determining the dispersion mechanisms in the

channel is rather challenging. In the following, a theoretical framework is proposed that aims, with some assumptions, to determine an approximated RTD for the different reactants involved in the synthesis.

To do so, we need to start from a physical description of the nanoparticles formation at a microscopic level. In a simplified picture, the liquid phase nanoparticles synthesis starts from one or more liquid reactants [30,31] that lead to the formation of nuclei through different mechanisms that depend on the synthesis considered. Nuclei size range typically between 1 and 20 *nm* in diameter. The nuclei formed then grow (through case-dependent mechanisms [31,32]) up to a final value. Thus, two different categories of reactants are involved in the process: the liquid-dissolved precursors and the growing particles. As already stated, the former are characterized by values of  $D_m$  generally close to  $10^{-9} \text{ m}^2/\text{s}$ , while the latter are characterized by values of  $D_m$  given by the Stokes-Einstein equation, which is valid for Brownian particles of spherical shape:

$$D_m = \frac{kT}{6\pi\mu R} \quad (2)$$

where  $k$  is the Boltzmann constant,  $T$  is the absolute temperature,  $\mu$  is the liquid viscosity and  $R$  is the particle radius. For  $R$  ranging between 1 and 100 *nm*, using values of temperature and viscosity characteristic of syntheses performed in aqueous phase, the Brownian diffusivity of the nanoparticles ranges between  $10^{-10}$  and  $10^{-12} \text{ m}^2/\text{s}$ . Thus, the nanoparticle diffusivity can be orders of magnitude smaller than that of the liquid reactants. Given the values of the fluid superficial velocity, reactor diameter and aspect ratio, it is evident that the aqueous reactants and the particles may not share the same RTD in the reactor, the former following the Taylor-Aris axial dispersion model, while the latter probably falling in the purely convective regime or in the transition regime [21]. Even when the fluid superficial velocity in the reactor is very low or the aspect ratio of the channel is very large, in a way that the nanoparticle RTD behave accordingly to the Taylor-Aris model, different values of  $D_{ax}$  will most likely characterize the nanoparticles and the liquid reactants, since  $D_{ax}$  depends on the molecular diffusivity [17].

Another aspect that needs to be considered is the variation of the nanoparticle diffusivity with the increase of its dimensions; Eq. (2) shows that the diffusivity scales with  $R^{-1}$ . From a general point of view, the particle growth is described by an increasing curve for the particle dimension against the time with an asymptote for  $t \rightarrow +\infty$ . For the sake of clarity, let us consider a growth curve of the type shown in Figure SI-1, without any loss in generality. This curve is characterized by an asymptote at  $d_\infty$ . The ratio  $d_\infty/d_{min}$  gives the order of magnitude of the maximum variation of the particle diffusivity. Here  $d_{min}$  represents the minimum nanoparticle size, that is, the size of the nuclei.

Even considering the significant deviations from a PFR just highlighted, we can reasonably assume as a first approximation that the particle size achieved by the LFR will be of *the same order of magnitude* as that achieved by a PFR. As a matter of fact, we can assume that every streamline will behave as a PFR with a velocity  $v(r)$ . Most of the streamlines will be characterized by values of velocity comparable to the average one, hence by a residence time of the order of magnitude of  $\tau$ . We can then initially consider the reactor output equivalent to that of a PFR; the variations of diffusivity during the reaction can then be easily analyzed. For a PFR, the average particle size output is  $d_p(\tau)$ , where  $\tau$  is the mean residence time of the reactor. Then, if the ratio  $G \equiv d_p(\tau)/d_{min} \approx 1$ , the variations in particle diffusivity along the reactor are negligible, and one can assume  $D_m = D_m(\tau)$  at any time. From the growth curve (see SI-1), we can define another important quantity: the characteristic time  $t^*$ . This is the time that the particle size requires to reach the order of magnitude of  $d_\infty$  during the growth process. For example, if  $d_\infty = 200 \text{ nm}$ , then  $t^*$  is the time required so that  $d(t^*) = 100 \text{ nm}$ . We can then consider the ratio  $\theta \equiv \tau/t^*$  between the mean residence time of the reactor and the characteristic time of the particle growth process. If  $\theta \ll 1$  (e.g.  $\approx 10^{-1} - 10^{-2}$ ) or  $\theta \gg 1$  (e.g.  $\approx 10 - 10^2$ ) one can infer that the effect of the diffusivity variation on the particle RTD is negligible as a first approximation. This is either because the particle size does not

significantly change during the process ( $\theta \ll 1$ ) or because the variation in the particle size is “localized” at the inlet reactor region ( $\theta \gg 1$ ). In both cases, one can assume  $D_m$  to be constant and equal to  $D_m(\tau)$ . A graphical representation of the described approximations is shown in Figure 1, where the regions highlighted represent those where the model developed in this work is applicable.

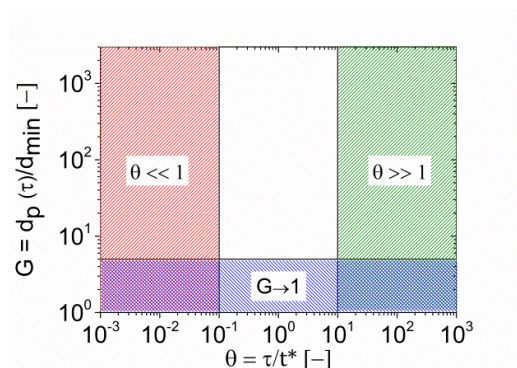


Figure 1 –  $G$  vs  $\theta$  plane describing the applicability of the constant diffusivity model. In the dashed regions the constant nanoparticle diffusivity assumption is applicable. When the size changes of the particles during the process are small ( $G = d_p(\tau)/d_{min} \approx 1$ ), or the mean residence time is much smaller ( $\theta = \tau/t^* \ll 1$ ) or larger ( $\theta = \tau/t^* \gg 1$ ) than the characteristic time of the diffusivity variations, then it is possible to neglect these variations when evaluating the RTD of the particles.

## 2.2 Two-phase Segmented Flow Reactors

Segmented flow reactors exploit Taylor flow to create “travelling batch reactors” inside a channel. When two fluid streams (either immiscible liquids or a gas and a liquid) are injected in capillaries, it is possible, under certain conditions, to achieve a regular pattern of alternating fluid slugs [20,33–35]. The continuous phase forms slugs which are connected by thin films in contact with the channel walls, while the disperse phase forms drops completely surrounded by the other phase. Which phase is continuous and which is disperse depends on the nature of the channel surface, specifically on its wettability with respect to the

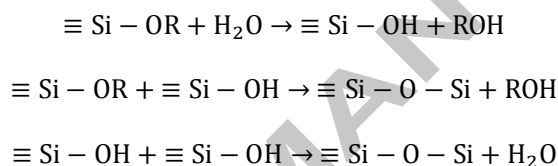
two fluids. The key dimensionless numbers characterizing this flow are the Capillary number  $Ca = \mu U / \sigma$  and the Weber number  $We = \rho U^2 l / \sigma$ , where  $\mu$  is the viscosity of the continuous phase,  $U$  is the velocity of the droplets,  $\sigma$  is the interfacial tension,  $\rho$  is the continuous phase density and  $l$  is the characteristic length scale of the tube (e.g. the tube diameter). Segmented flow can be easily obtained in microchannels, because their characteristic dimension approaches the Laplace scale, so that the interfacial forces become dominant [20]. A relevant effect of the interfacial forces is the presence of a slip velocity at the boundary between the two phases. This slip velocity, whose magnitude depends on the nature of the fluids involved [33], causes circulation patterns into the slugs [36], improving radial mass transfer.

When stable slug patterns are achieved, the RTD for these reactors is close to that of a PFR [29,33], with small deviations observed. These deviations are more relevant when the reactive fluid is the continuous phase, and are mostly influenced by the dimensions of the slugs and by the thickness of the wetting film in contact with the reactors walls, which represent the main source of axial dispersion [37]. Furthermore, if the reactor is designed to guarantee good mixing of the reactants before the injection of the segmenting fluid [19] and if an intense circulation inside the reacting drops is guaranteed, it can be inferred that the effect of the reactant diffusivity on the RTD is negligible. When this assumption is valid, these reactors can be regarded as ideal PFRs as a first approximation, and the diffusivity mismatch between particles and precursors, highlighted for the LFR in the previous section, does not play a role in reactor performance.

We now apply the above framework to a case study. Khan et al. [19] synthesized colloidal silica through the Stöber process in continuous flow microreactors with different flow conditions, and compared the results to those obtained in a batch reactor. They highlighted how the syntheses performed in the single-phase reactor led to smaller and more disperse particles compared to the synthesis performed in batch reactors, and suggested how this phenomenon could be ascribed to RTD-effects. On the other hand, the segmented-flow reactor, when optimally designed, leads to particle distributions equivalent to those of the batch process.

### 3. Stöber process kinetics

The Stöber process is a chemical synthesis yielding uniform silica nanoparticles ( $\text{SiO}_2$ ) from tetraethyl orthosilicate (TEOS) as precursor, in a mixture of water, and a short chain alcohol (typically methanol or ethanol), with ammonia as catalyst. The process is extensively characterized and several mechanistic studies are available in the literature [38–45], which generally involve a series of hydrolysis and condensation reactions, which can be summarized as follows [39]:



The LaMer model [46] for the kinetics of formation of hydrosols is generally used as a reference framework for mechanistic studies on nanoparticles formation [32]. Nevertheless, deviations from this theory have been observed [31]. To describe the Stöber process, the most accepted model is that proposed by Bogush and Zukoski [39], which is an aggregative model: silica nuclei are formed during the whole process by the hydrolysis of TEOS, which is a slow process even when catalyzed; the nuclei then grow through a size-dependent aggregative process which leads to uniformity in the size of the particles.

With this picture in mind, different authors used population balance equations to describe the evolution of the particle size distribution in batch reactors under different operating conditions [39,47,48]. Eq. (3) shows the population balance equation describing the Stöber process (in a batch reactor assumed to be well mixed, so that all intensive variables are uniform), where only the nucleation and aggregation terms are present (Eq. (3) is described in the Supplementary Information, SI-2):

$$\begin{aligned} \frac{\partial n(R, t)}{\partial t} = & g\delta(R - R_{min}) + \frac{R^2}{2} \int_{R_{min}}^R \frac{q[\tilde{R}(R, R'), R']}{\tilde{R}(R, R')^2} n[\tilde{R}(R, R'), t] n(R', t) dR' \\ & - n(R, t) \int_{R_{min}}^{+\infty} q(R, R') n(R', t) dR' \end{aligned} \quad (3)$$

where  $n(R, t)$  is the number density of the particles with radius  $R$  at time  $t$  (so that  $n(R, t)dR$  yields the number of particles with size in the range  $dR$  around  $R$ ),  $\delta(R - R_{min})$  is the Dirac delta function centered on the nuclei radius  $R_{min}$  (all nuclei are assumed to have the same size) and  $q$  is the aggregation kernel between two particles,  $g$  is the nucleation rate.  $R'$  is a dummy integration variable and  $\tilde{R}(R, R')$  is given by:

$$\tilde{R}(R, R') = (R^3 - R'^3)^{1/3} \quad (4)$$

No particles are present in the system at  $t = 0$  s, while the concentration of TEOS is set as  $[\text{TEOS}](t = 0) = [\text{TEOS}]_0$ . The first term on the right-hand side of Eq. (3) represents the nucleation term, while the second and third terms represent the aggregation between particles, as described by the Smoluchowski coagulation model. To take into account DLVO interactions between particles [31,49], the aggregation kernel  $q$  is written as:

$$q(R, R') = \frac{q_B(R, R')}{W(R, R')} \quad (5)$$

where  $q_B(R, R')$  is the Brownian aggregation kernel defined as:

$$q_B(R, R') = \frac{2kT}{3\mu} (R + R') \left( \frac{1}{R} + \frac{1}{R'} \right) \quad (6)$$

and  $W(R, R')$  represents the stability factor [49][31] for the interaction between two particles of radii  $R$  and  $R'$ , and is expressed as:

$$W(R, R') = (R + R') \int_{R+R'}^{+\infty} (1/\delta^2) \exp \left[ \frac{V_T(\delta, R, R')}{kT} \right] d\delta \quad (7)$$

where  $\delta$  is the distance between the particles surfaces and  $V_T(R, R')$  is the total interaction potential between the two particles of radii  $R$  and  $R'$ .

The total interaction potential between the two particles consists of three contributions: van der Waals attractive interaction, electrostatic repulsion and solvation repulsion. The van der Waals attractive potential is given by:

$$V_{VDW}(\delta, R, R') = -\frac{A_H}{6} \left[ \frac{2RR'}{\delta^2 - (R + R')^2} + \frac{2RR'}{\delta^2 - (R - R')^2} + \ln \left( \frac{\delta^2 - (R + R')^2}{\delta^2 - (R - R')^2} \right) \right] \quad (8)$$

where  $A_H$  is the Hamaker constant. The electrostatic repulsion potential can be expressed as [49]:

$$V_E(\delta, R, R') = 4\pi\epsilon_0\epsilon_r\psi_0^2 \left( \frac{2RR'}{R + R'} \right)^2 \frac{\exp[-\kappa(\delta - R - R')]}{\delta} \quad (9)$$

where  $\epsilon_0$  is the vacuum permittivity,  $\epsilon_r$  is the relative permittivity of the solution,  $\psi_0$  is the surface electric potential and  $\kappa$  is the inverse Debye length. The solvation repulsion potential is given by [39]:

$$V_s(\delta, R, R') = \pi A_s l \frac{2RR'}{R + R'} \exp\left(-\frac{\delta - R - R'}{l}\right) \quad (10)$$

where  $A_s$  is a pre-exponential factor and  $l$  is the decay length. Owing to the large number of values for  $R$  and  $R'$ , solving Eq. (7) when simulating the evolution of the particle size distribution is computationally demanding; an alternative approach is to employ the Reerink and Overbeek approximation [50]. These researchers showed that the integral in Eq. (7) is dominated by the maximum value of the potential, and can be approximated as:

$$W(R, R') = \frac{K}{R + R'} \exp\left(\frac{V_m}{kT}\right) \quad (11)$$

where  $K$  is a proportionality constant and  $V_m$  is the maximum of the interaction potential. In Figure 2 the mentioned potential as a function of the surface-surface distance between the particles is sketched. The peak value  $V_m$  is clearly recognizable (for the values of the parameters used to compute the potential see Table 2).

Bogush and Zukoski [39] showed that it is possible to express the maximum potential between two interacting particles  $i$  and  $j$  as a function of their effective radius  $R_{ij} = 2R_i R_j / (R_i + R_j)$ , considering the potential peak as a linear increasing function of the effective radius, so that Eq. (11) can be rewritten as:

$$W(R, R') = \frac{K}{R + R'} \exp\left(J \frac{2RR'}{R + R'}\right) \quad (12)$$

where  $J$  is the proportionality constant between the maximum potential and the effective radius.

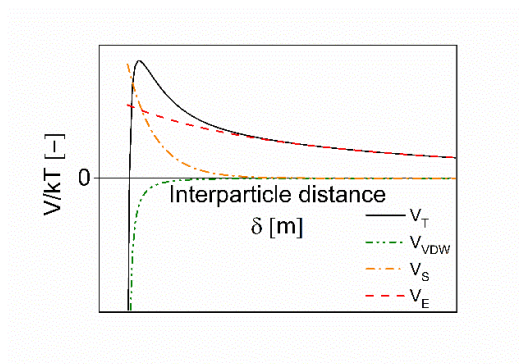


Figure 2 – Sketch of the interaction potentials as a function of distance between the particles.  $V_T$  is the total interaction potential, given by the sum of the van der Waals potential  $V_{VDW}$ , the solvation potential  $V_S$  and the electrostatic potential  $V_E$ .

Kim and Zukoski [51] showed that a better approximation for the stability factor is obtained when it scales with  $R^{-2}$ ; hence, the final formulation employed to express the stability factor is given by:

$$W(R, R') = \frac{K}{(R + R')^2} \exp\left(J \frac{2RR'}{R + R'}\right) \quad (13)$$

Several studies [38,39,47,48] showed that the nucleation rate  $g$  in Eq. (3) can be expressed as a function of the rate of conversion of TEOS, which is well approximated by a first-order kinetics:

$$r_{\text{TEOS}} = -k_n[\text{TEOS}] \quad (14)$$

where  $k_n$  is the kinetic constant of TEOS conversion.

Hence,  $g$  can be expressed as:

$$g(t) = \frac{v_M}{v_{min}} k_n [\text{TEOS}]_0 \exp(-k_n t) \quad (15)$$

where  $v_M$  is the molar volume of solid silica,  $v_{min}$  is the volume of a silica nucleus and  $[\text{TEOS}]_0$  is the initial concentration of TEOS.

Even though kinetic parameters are available in the literature [39,47,48], the reaction conditions do not exactly match those of the experiments used in this work. Thus, in the following we calculate these parameters by fitting the batch kinetic data. Khan et al. [19] performed this synthesis in an ethanol solution with ammonia as catalyst, with two different sets of reactant concentrations: experiment set (A)  $[\text{TEOS}] = 0.1 \text{ M}$ ,  $[\text{NH}_3] = 1 \text{ M}$ ,  $[\text{H}_2\text{O}] = 13 \text{ M}$  and experiment set (B)  $[\text{TEOS}] = 0.2 \text{ M}$ ,  $[\text{NH}_3] = 2 \text{ M}$ ,  $[\text{H}_2\text{O}] = 5.9 \text{ M}$ . Their batch results were fitted to obtain the parameters of the kinetic model, reported in Table 1.

Experiment	$J$	$K$	$k_n$
Set	( $\text{nm}^{-1}$ )	( $\text{m}^2$ )	( $\text{s}^{-1}$ )
(A)	0.35	$2.0 \cdot 10^{-18}$	$1.0 \cdot 10^{-3}$
(B)	0.26	$1.5 \cdot 10^{-18}$	$8.0 \cdot 10^{-4}$

Table 1 – List of fitted parameters obtained from the batch synthesis modelling. Other parameters required to compute the simulations are  $R_{min} = 10 \text{ nm}$  (with  $v_{min} = 4/3\pi R_{min}^3$ ) and  $v_M = 2.7 \cdot 10^{-5} \text{ mol m}^{-3}$ .

The parameters required to solve Eq. (3) are  $J$ ,  $K$ ,  $k_n$ ,  $R_{min}$  and  $v_M$ , with  $W$  given by Eq. (13) and  $g$  by Eq. (15). The values of  $R_{min}$  and  $v_M$  were taken from the literature [44,48], while  $K$  and  $k_n$  have been treated as fitting parameters. Regarding  $J$ , a different approach was followed for the two experiment sets:

- Experiment Set (*A*): this set is characterized by values of reactants concentrations in the range of the kinetics studies available in the literature [39,47,48]. Hence the approach based on the evaluation of the interaction potentials was followed: in order to calculate the parameter  $J$ , the total potential was calculated from Eqs. (8)-(10) for a number of ( $R, R'$ ) combinations. Then, the maximum values of the total interaction potential obtained for each ( $R, R'$ ) combination were fitted with a linear function of the effective radius:

$$\frac{V_m(R, R')}{kT} = J \frac{2RR'}{R + R'} \quad (16)$$

The values of the parameters required to compute the total potential were taken from the literature, as reported in Table 2.

$k$	$T$	$\mu$ [48]	$\rho$ [48]	$A_H$ [39,47,48]	$\epsilon_0$	$\epsilon_r$ [39,47,48]
( $\text{m}^2 \text{kg s}^{-2} \text{K}^{-1}$ )	(K)	(Pa s)	( $\text{kg m}^{-3}$ )	(J)	(F m)	
$1.38 \cdot 10^{-23}$	300	$1.5 \cdot 10^{-3}$	850	$1.0 \cdot 10^{-20}$	$8.85 \cdot 10^{-12}$	35

$\psi_0$ [47,48]	$\kappa$ [39]	$A_s$ [39,47]	$l$ [39,47]
(mV)	( $\text{m}^{-1}$ )		(m)
-30	$3 \cdot 10^7$	$1.5 \cdot 10^{-3}$	$1.0 \cdot 10^{-9}$

Table 2 – List of parameters used to compute the interparticle interaction potentials for Experiment Set (*A*).

- Experiment Set (*B*): since the reactant concentrations used for this experiment set differ significantly from those reported in the kinetics studies available in the literature, in this case  $J$  was

treated as a fitting parameter, retrieved through the fitting of the experimental average size and relative standard deviation. Note that the value obtained for experiment set (*B*) is of the same order of magnitude as that obtained for experiment set (*A*) from a more rigorous physical approach (see Table 1).

To sum up, for the Experiment Set (*A*) the only fitting parameters used were  $K$  and  $k_n$ . These were tuned in order to best reproduce the experimental data. Note that the value of  $k_n$  is in good agreement with those reported in the literature, ranging between  $1 \cdot 10^{-4} s^{-1}$  and  $2 \cdot 10^{-3} s^{-1}$  [38,39,47,48]. For the Experiment Set (*B*), all the three parameters  $J, K, k_n$  were treated as fitting quantities, tuned to fit the average size of the population. The values of the parameters obtained for Experiment Set (*B*) were of the same order of magnitude as those used for set (*A*) (Table 1). The fitting procedure is explained in the Supplementary Information SI-3.

The results obtained from the solution of the population balance equation with the fitted parameters are compared with the data by Khan et al. [19] in Figure 3 (average particle size and relative standard deviation measured from TEM images obtained after casting a drop of the colloidal solution collected at the reactor outlet on a carbon coated 200-mesh grid). Good agreement between the model results and the experimental data is observed in terms of average particle size  $\bar{d}$  (maximum deviation in the order of 5%). The relative standard deviation of the particle size distribution  $rsd = \sigma/\bar{d}$  (with  $\sigma^2$  variance of the particle size distribution) obtained from the model overestimates the experiments, in particular for low values of the reaction time. This may be due to the fact that the parameters needed to calculate the various potentials in Eqs. (10)-(12) depend on the chemical composition of the system and on the particle size [47,52]. Consequently,  $J$  should be a function of time as well. In the present work, this dependency is neglected, due to lack of relevant experimental data, whose measurement is not trivial. This approximation may lead to deviations from the experimental measurements, especially in the first part of the reaction,

where the changes in the particle size and in the chemical composition of the system are more marked. Still, the model provides a satisfactory fitting of the experimental data.

Qualitatively, from the graph in Figure 3 one can observe the increase of the particles size in time due to the aggregation between the particles, as well as a decrease in the relative standard deviation. This last point may seem counterintuitive, and is due to the dependency of the stability factor  $W$  on the aggregating particles radii combined with the peculiar physiochemical composition of the reactive mixture. As previously pointed out, TEOS conversion continues throughout the whole reaction, constantly providing nuclei to the reaction mixture. Monodispersity of the particle size distribution is achieved through a size-dependent aggregation rate. The physical chemistry of the system is such that larger particles stop aggregating with each other and grow by scavenging the nuclei provided by TEOS throughout the whole reaction [39] (see SI-4).

Comparing the two sets of experiments, set A led to smaller particles than set B. This is consistent with what is reported in the literature [40,47]: first, the increase in ammonia concentration is reported to increase the average particle size; furthermore, experiments carried out with varying water concentration show a peak for the average dimension of the particles at a concentration of water in the range of 5 M (as in protocol B). These trends are reported to be due to a decrease in the nucleation rate, which is also observed from our fitted parameters (see Table 1).

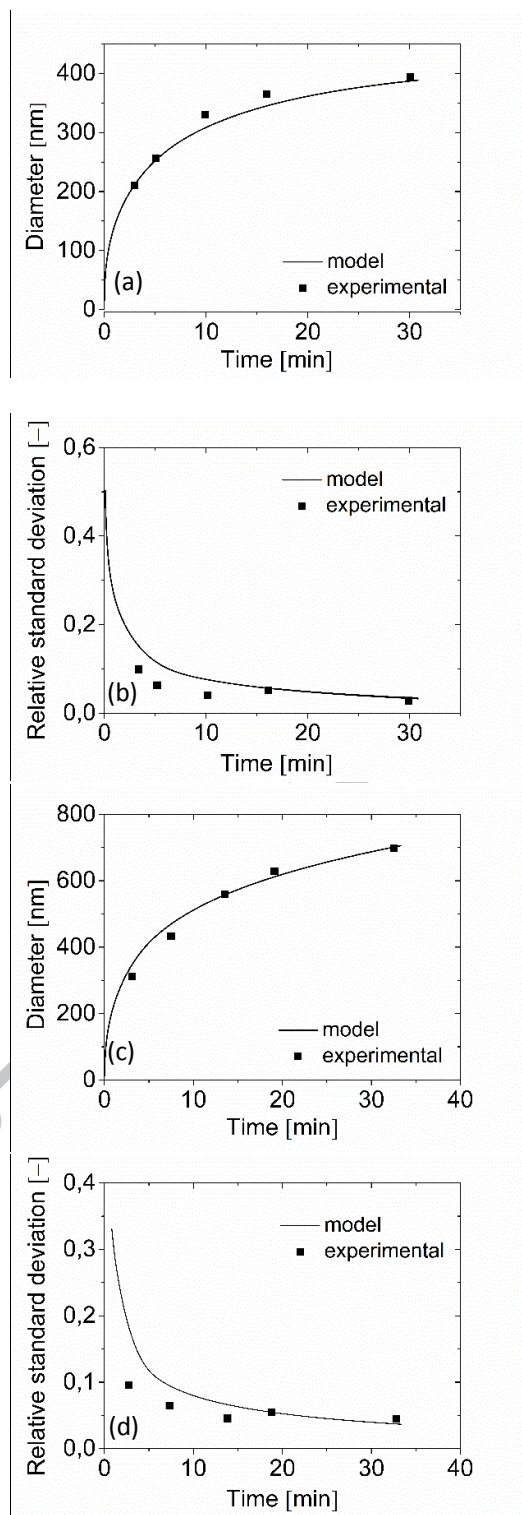


Figure 3 – Results of the modelling of the batch experiments of Khan et al. [19] (a) average particle diameter for Experiment Set (A) (b) relative standard deviation for Experiment Set (A), (c) average particle diameter for Experiment Set (B), (d) relative standard deviation for Experiment Set (B); error bars are not reported in the original work.

## 4. Continuous synthesis of Silica Nanoparticles

### 4.1 Single-phase Laminar Flow Reactor

Khan et al. [19] performed synthesis (A) (as described in Section 3) with a continuous approach, using a microreactor composed of two sections: a mixing part with a cross section  $50 \mu\text{m}$  wide,  $150 \mu\text{m}$  deep and a length of  $40 \text{ mm}$ , and an aging part  $400 \mu\text{m}$  wide,  $150 \mu\text{m}$  deep with a length of  $0.975 \text{ m}$ . Aubin et al. [53] and Wörner [54] investigated the effect of the cross section aspect ratio on the RTD in rectangular cross section channels by means of CFD simulations and showed that for cross section aspect ratios above 0.25 the RTD of these channels is almost equivalent to that of the corresponding circular section channels, with the best matching for an aspect ratio of the section equal to 0.5. For the reactor studied here, the cross section aspect ratio is 0.375, hence in the following we assume the reactor to be equivalent to a cylinder characterized by a hydraulic diameter  $d_t = 218 \mu\text{m}$ .

In their work, Khan et al. [19] tested different residence times, and observed smaller and more dispersed particles formed during the continuous synthesis, compared to the products of the corresponding batch synthesis.

We applied the framework developed in Section 2.1 to model these results. First, an analysis on the variability of the particle diffusivity was carried out. From the results of the batch synthesis modelling (Section 3) the characteristic time of the particle growth process was calculated as  $t^* \approx 24 \text{ s}$  by imposing  $d(t^*) = 100 \text{ nm}$ . To further support this result, we analyzed the change of the particle diffusivity with

time. In Section 3 we obtained the average radius of the nanoparticles  $R$  as a function of time. Then, we substituted  $R(t)$  in the Stokes-Einstein equation (Eq.(2)), which describes the particle Brownian diffusivity as a function of its radius. In this way we obtained the curve  $D_m(t)$ , reported in Figure 4. One can observe that the diffusivity drops to an approximately constant value after roughly 24 s; the value of  $t^* \approx 24$  s then results to be a reasonable choice for the diffusivity variation analysis.

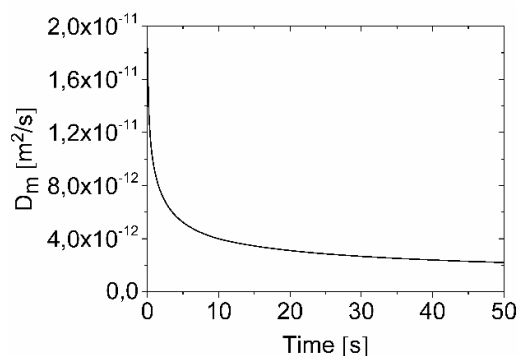


Figure 4 – Particle Brownian diffusivity as a function of time during the reaction. The decrease is due to the increase of the average particle size during the synthesis.

While  $G \gg 1$  in all the experiments performed by Khan et al. [19], the ratio  $\theta$  ranged between 7.5 for the lowest residence time of 3 min to 75 for the highest residence time of 30 min. The validity of the constant diffusivity approach is then rigorously verified only at high residence times. In order to determine the RTD of the particles, the value of  $D_m(t = \tau)$  was used for all the experiments considered (approximately equal to  $2 \cdot 10^{-12} m^2/s$ ), while for the precursor a value of  $D_m = 10^{-9} m^2/s$  was used.

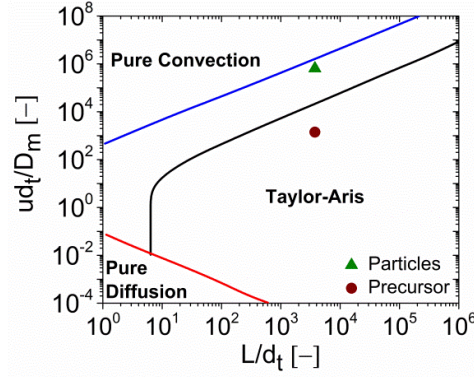


Figure 5 – Residence Time Distribution determination for particles and precursor at  $\tau = 3 \text{ min}$ .

As shown in Figure 5, for the precursor, the Taylor-Aris axial dispersion model should be applied, leading to a value of  $D_{ax}/uL < 0.01$  for all residence times modeled, confirming the validity of the PFR model [17]. For the particles, even though for all the residence times tested the Figure suggests that none of the models is completely correct, the proximity to the convective region suggests the applicability of the pure convection model. Furthermore, deriving the RTD in the transition region does not generally bring a significant improvement of the results [17]. According to the purely convective model, the particles average motion is limited to the sole streamline where they initially belong; hence poor micromixing is present in the particle phase. This condition of poor micromixing is taken into account in the following by the use of a maximally segregated approach [17] in the calculation of the particle size distribution moments.

The system of equations that needs to be solved is then:

$$\begin{cases} \frac{Dn(R, r, z)}{Dt} \equiv v(r) \frac{\partial n(R, r, z)}{\partial z} = r_{stober}(R, r, z) \\ u \frac{d[\text{TEOS}](z)}{dz} = r_{\text{TEOS}}(z) \end{cases} \quad (17)$$

where  $v(r)$  is the parabolic velocity profile characteristic of the laminar flow in a cylindrical tube,  $v(r) = 2u[1 - (r/r_t)^2]$ ,  $r$  is the radial coordinate in the channel,  $r_t$  is the tube radius,  $r_{stober}$  is the right-hand side term of the population balance equation (3) and  $r_{\text{TEOS}}$  is the rate of TEOS conversion (equation

(14)) (see Supplementary Information SI-5 for an extended description of Eqs. (17)). No silica particles enter the reactor at  $z = 0$  (that is,  $t = 0$ ), while the concentration of TEOS at the reactor inlet is set as  $[\text{TEOS}](z = 0) = [\text{TEOS}]_0$ .

Eqs. (17) are decoupled, since the second one (TEOS mass balance) does not depend on the particle size distribution. The TEOS mass balance can easily be solved, obtaining:

$$[\text{TEOS}] = [\text{TEOS}]_0 \exp\left(-\frac{k_n z}{u}\right) \quad (18)$$

Substituting Eq. (18) in the first equation in (17), we obtain:

$$\begin{aligned} v(r) \frac{\partial n(R, r, z)}{\partial z} &= \frac{v_M}{v_{min}} k_n [\text{TEOS}]_0 \exp\left(-\frac{k_n z}{u}\right) \delta(R - R_{min}) \\ &+ \frac{R^2}{2} \int_{R_{min}}^R \frac{q[\tilde{R}(R, R'), R']}{\tilde{R}(R, R')^2} n[\tilde{R}(R, R'), r, z] n(R', r, z) dR' \\ &- n(R, r, z) \int_{R_{min}}^{+\infty} q(R, R') n(R', r, z) dR' \end{aligned} \quad (19)$$

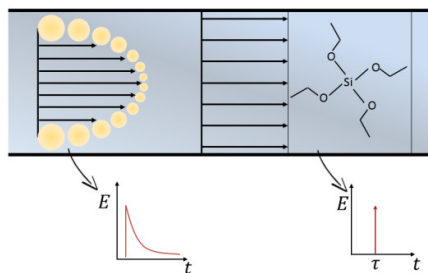


Figure 6 – Sketch of the different transport phenomena involving the particles (left) and TEOS (right) in the single-phase reactor, and their effect on the RTDs. The arrows represent the velocities at which each component of the reaction mixture is moving. As a result, particles and precursor do not share the same RTD.

For a given value of  $r$ , Eq. (19) describes a PFR characterized by a superficial velocity  $v(r)$ . It is then possible to solve this equation for each value of  $r$ , determining a particle size distribution  $n(R, r, z)$ . Rather than solving the equation in the space domain, using the variable transformation  $t = z/v(r)$ , we find it more convenient to solve the following equation in the time domain, written from the point of view of an observer that moves with the particles contained in a differential fluid element:

$$\begin{aligned} \frac{\partial n(R, r, t)}{\partial t} = & \frac{v_M}{v_{min}} k_n [\text{TEOS}]_0 \exp\left(-\frac{k_n v(r) t}{u}\right) \delta(R - R_{min}) \\ & + \frac{R^2}{2} \int_{R_{min}}^R \frac{q[\tilde{R}(R, R'), R']}{\tilde{R}(R, R')^2} n[\tilde{R}(R, R'), r, t] n(R', r, t) dR' \\ & - n(R, r, t) \int_{R_{min}}^{+\infty} q(R, R') n(R', r, t) dR' \end{aligned} \quad (20)$$

from which, one can obtain for every streamline the number density function  $n(R, r, t)$ . At the outlet of the reactor, the time and the radial coordinate are functionally related through the equation  $t = L/v(r)$ , which when solved with respect to  $r$ , gives:

$$r(t) = r_t \sqrt{1 - \frac{L}{2ut}} \quad (21)$$

In the purely convective model, the RTD is equal to:

$$E(t) = \frac{\tau^2}{2t^3} H\left(t - \frac{\tau}{2}\right) \quad (22)$$

where  $H(t - \tau/2)$  is the step function with the discontinuity located at  $t = \tau/2$  [17].

We can then define an average number density function for the particle population at the reactor outlet:

$$\bar{n}(R) = \int_0^{+\infty} n[R, r(t), t] E(t) dt \quad (23)$$

which represents the actual output of the reactor.

It is possible to use the same approach on the moments of the two distributions. Next we define the number of particles, average size and variance for both distributions  $n(R, r(t), t)$  and  $\bar{n}(R)$  as:

$$\bar{N}(t) = \int_0^{+\infty} n[R, r(t), t] dR \quad (24)$$

$$\bar{R}(t) = \frac{\int_0^{+\infty} R n[R, r(t), t] dR}{\bar{N}(t)} \quad (25)$$

$$\bar{\sigma}^2(t) = \frac{\int_0^{+\infty} [R - \bar{R}(t)]^2 n[R, r(t), t] dR}{\bar{N}(t)} \quad (26)$$

$$\bar{\bar{N}} = \int_0^{+\infty} \bar{n}(R) dR \quad (27)$$

$$\bar{R} = \frac{\int_0^{+\infty} R \bar{n}(R) dR}{\bar{N}} \quad (28)$$

$$\bar{\sigma}^2 = \frac{\int_0^{+\infty} (R - \bar{R})^2 \bar{n}(R) dR}{\bar{N}} \quad (29)$$

Here  $\bar{N}(t)$ ,  $\bar{R}(t)$  and  $\bar{\sigma}^2(t)$  are the number density of particles, the average size and the variance for the distribution  $n(R, r, t)$ , while  $\bar{N}$ ,  $\bar{R}$  and  $\bar{\sigma}^2$  represent the same quantities for the distribution  $\bar{n}(R)$ .

Using Eqs. (24) – (29), it is possible to demonstrate the following relationships between the moments of the two distributions (see Supplementary Information SI-6):

$$\bar{N} = \int_0^{+\infty} \bar{N}(t) E(t) dt \quad (30)$$

$$\bar{R} = \frac{1}{\bar{N}} \int_0^{+\infty} \bar{N}(t) \bar{R}(t) E(t) dt \quad (31)$$

$$\bar{\sigma}^2 = \frac{1}{\bar{N}} \int_0^{+\infty} \bar{N}(t) [\bar{\sigma}^2(t) + \bar{R}(t)^2] E(t) dt - \bar{R}^2 \quad (32)$$

Eq. (20) was solved for several streamlines ( $\Delta r = 0.01 r_t$  until the average size of the population did not change for more than 1% between two consecutive streamlines), leading to  $n(R, r, t)$ , from which one can

obtain  $\bar{N}(t)$ ,  $\bar{R}(t)$  and  $\bar{\sigma}^2(t)$ . Then, the average size and relative standard deviation of the particle size distribution  $\bar{n}(R)$  at the reactor outlet were calculated using Eqs. (30)-(32).

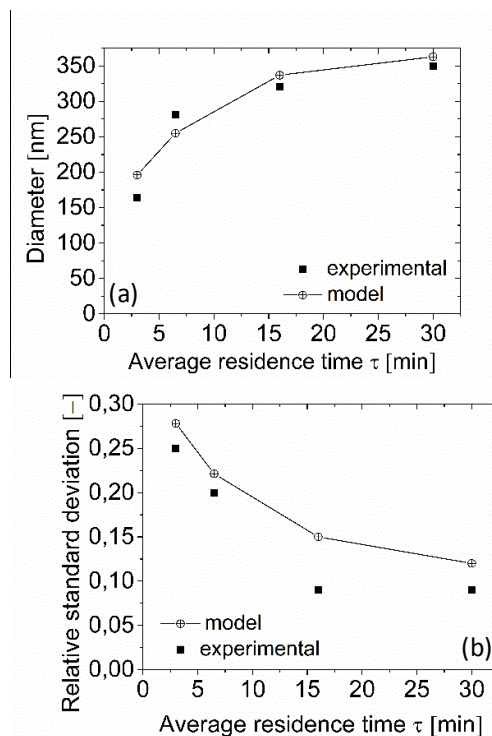


Figure 7 – Comparison between experimental [19] and modeled data for single phase laminar flow reactor (LFR) employed to synthesize silica nanoparticles according to Experiment Set (A). (a) Average particle diameter,  $2\bar{R}$ , (b) Relative standard deviation,  $\bar{\sigma}/\bar{R}$ , obtained at various average residence times.

The results are shown in Figure 7, where it is possible to see that the proposed model is able to predict reasonably well the reactor output in terms of average particle size and standard deviation of the particle size distribution. As regards the average particle size, the error in the prediction for the lowest residence time ( $\tau = 3 \text{ min}$ ) is rather high ( $\approx 19\%$ ) but rapidly drops for the following residence time of  $\tau = 6.5 \text{ min}$  ( $\approx 9\%$ ), gradually decreasing when  $\tau$  increases, down to  $\approx 3\%$  for  $\tau = 30 \text{ min}$ . It is possible that this is due to the increasing validity of the constant diffusivity hypothesis for the particles, since the ratio  $\theta$  significantly increases when  $\tau$  increases. The error for the relative standard deviation is larger, with the

model overestimating the relative standard deviation by about 10%, except for  $\tau = 16 \text{ min}$ , where it reaches 50 %. Furthermore, the error on the relative standard deviation seems not to follow a trend. Note that the only fitting parameters used in the entire modeling of the LFR are the constants  $K$  and  $k_n$ , used to fit the batch reactor data.

## 4.2 Two-phase Segmented Flow Reactor

In Section 2.2 it was pointed out that, with proper design, SFRs can behave as an ideal PFR. This means that it is possible to exploit the equivalence between batch reactors and PFRs:  $t_{batch} \leftrightarrow \tau_{PFR}$ . It is indeed possible to neglect the small deviations from PFR [17] (Figure 8) and assume for these reactors an RTD in the form of:

$$E(t) = \delta(t - \tau) \quad (33)$$

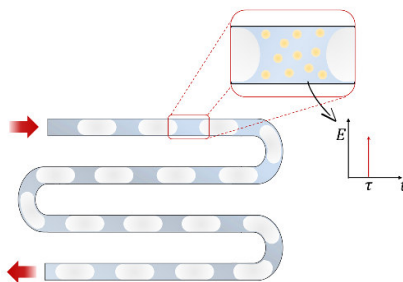


Figure 8 – Sketch of the SFR. Flow segmentation leads to the formation of “travelling batches” where the particle synthesis takes place, with a significant reduction of the RTD spread.

Recalling Eq. (23), the particle size distribution at the reactor outlet is given by:

$$\bar{n}(R) = \int_0^{+\infty} n(R, t)E(t)dt \quad (34)$$

Here, the dependence of  $n$  on the reactor radial coordinate  $r$  (reported in Eq. (23)) is removed, since the PFR approximation is adopted, hence no effect of the radial coordinate is present.

Substituting Eq. (33) in Eq. (34) one obtains:

$$\bar{n}(R) = n(R, \tau) \quad (35)$$

From Eqs. (30)-(32), it is easy to demonstrate that similar relations exist between the moments of the two particle size distributions  $\bar{n}(R)$  and  $n(R, t)$ . Recalling the notation used in Section 4.1, we obtain:

$$\bar{\bar{N}} = \bar{N}(\tau) \quad (36)$$

$$\bar{\bar{R}} = \bar{R}(\tau) \quad (37)$$

$$\bar{\bar{\sigma}} = \bar{\sigma}(\tau) \quad (38)$$

The approach adopted is similar to that used by Lazzari et al. [13], who modeled the formation of semiconductor nanocrystals in a droplet-based microreactor; their model is based on the use of population balance equations where the effect of residence time distributions is neglected. Their results agree with the experiments from Abolhasani et al. [55], who performed the synthesis in a droplet-based reactor.

Khan et al. [19] performed the synthesis of silica nanoparticles using a microfluidic device with an air-liquid segmented flow pattern. In their device, the reaction takes place in the continuous phase; this may

introduce some deviations between the proposed model and the experimental data, owing to the axial dispersion caused by the wetting film (as pointed out in Section 2.2). The chemistry used was described in Section 3 as experiment set (B). The batch data were reproduced with the aid of population balance equations in the same section (Figures 3 (c) and (d)). Figure 9 reports the comparison between batch and flow (SFR) synthesis, as well as the model results described in Section 3.

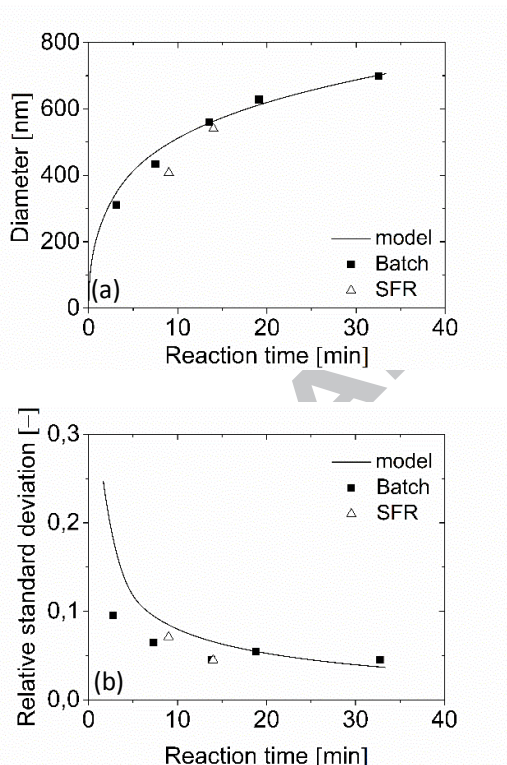


Figure 9 – Comparison between experiments [19] and model for batch reactor and segmented flow reactor (SFR) employed to synthesize silica nanoparticles according to Experiment Set (B). (a) Average particle diameter,  $2\bar{R}$ , (b) Relative standard deviation  $\bar{\sigma}/\bar{R}$ , obtained at various reaction times (which is  $\tau$  in case of the SFR).

The model predicts satisfactorily the nanoparticle average size evolution, while less agreement is found for the standard deviation of the size distribution, particularly in the first stage of the synthesis, as also pointed

out in Section 3. This limitation can be ascribed to the kinetic model employed, which shows a better agreement with experimental data in terms of average size rather than standard deviation.

The model prediction exploits a set of fitting parameters determined directly from the batch syntheses. The model is nevertheless able to reasonably predict the segmented flow system as well (without the necessity of modifying the fitting parameters). In other words, the knowledge of the time-evolution of the particle size distribution from batch experiments allows predicting the output of the reactor. Note that the design of these devices is still challenging since a regular slug pattern must be produced to obtain these results.

It is important to point out that batch synthesis may be affected by lack of homogeneity in the reactor, due to poor mixing conditions, particularly in the case of large batch reactors. When properly designed, Segmented Flow Reactors overcome these limitations, allowing a more reproducible synthesis, as pointed out in the literature [22,56], and possibly leading to even more monodispersed particles than the batch counterpart.

#### 4.3 Flow-induced deviations from batch processes: the influence of diffusion phenomena on nanoparticle growth

In this section we comment on the effect of the mismatch in the dispersion mechanism between the precursor and the particles in the single-phase Laminar Flow Reactor on the nanoparticle growth process.

From Eq. (20) we can observe how the TEOS concentration influences the particle formation only in the nucleation step. The nucleation term in the equation is:

$$g = \frac{v_M}{v_{min}} k_n [\text{TEOS}]_0 \exp \left[ -\frac{k_n v(r) t}{u} \right] \quad (39)$$

This term differs from that reported in Eq. (15) (batch synthesis) due to the presence of the ratio  $v(r)/u$  in the exponential. This term disappears if nanoparticles and precursor share the same RTD (as in the SFR). The ratio varies from streamline to streamline, assuming values above or below one. This leads to an *apparent* nucleation constant in the exponential:

$$g = \frac{v_M}{v_{min}} k_n [\text{TEOS}]_0 \exp[-k_a(r)t] \quad (40)$$

where  $k_a(r) = k_n v(r)/u$ . This new *apparent* nucleation constant  $k_a$  is higher than  $k_n$  on the central streamlines, where  $v(r) > u$ , and lower than  $k_n$  on the peripheral streamlines, where  $v(r) < u$ . The former leads to smaller particles than expected if no mismatch in the RTD were taken into account, while the latter to bigger particles. This is a source of further deviations from the ideal PFR model, which a simple averaging procedure over the RTD would not have accounted for. It is important to highlight how the effects of the diffusion mismatch between the particles and the liquid phase precursor on the reactor output differ from synthesis to synthesis, depending on the type of interaction between the particles and the precursor involved in the reaction (e.g. nucleation rate, surface growth etc.), which changes depending on the reaction mechanism [30,31]. Consequently, due to these diffusion phenomena single-phase reactors may even lead to larger nanoparticles than those produced in comparable batch processes, a phenomenon that cannot be explained by a simple averaging procedure of the batch growth curve on the RTD of the reactor. The highlighted mismatch in the dispersion mechanism between precursor and nanoparticles represents a further cause of deviation from an ideal PFR reactor, and can also be suggested as one of the reasons for the observed difficulty in the comparison between different experimental set-ups, since the dispersion mechanisms are strongly affected by the geometry of the reactor [17]. This phenomenon is not observed in the SFRs, in which the intense convective recirculation inside the reactive slugs forces the particles and the liquid precursor to share the same dispersion conditions.

## 5. Conclusions

This work presents a model for the liquid-phase synthesis of nanoparticles in two common classes of continuous milli- and micro-reactors, namely single-phase Laminar Flow Reactors and two-phase Segmented Flow Reactors. The model is built on the RTD-based classic reaction engineering approach, in which the deviations from ideal flow conditions are taken into account by introducing distribution functions for the fluid residence times, so that the real residence time in the reactor of each fluid element is considered. To identify the conditions of validity of this approach, the characteristic growth curve of the particles was analyzed, and two dimensionless groups were proposed to describe the relevance of the particle Brownian diffusivity variation during the synthesis. These two groups are  $G = d_p(\tau)/d_{min}$  (ratio between the average particle size evaluated at the mean residence time and the nuclei size) and  $\theta = \tau/t^*$  (ratio between the mean residence time and the characteristic time of the particle growth). The proposed analysis leads to the determination of the proper RTDs for the evaluation of the reactor output. The reaction kinetics employed in the modelling of the flow syntheses was described with the aid of population balance modelling. The kinetics, derived from batch experiments, were used to model the flow syntheses, without any adjustable parameter. The model was employed to describe the synthesis of silica nanoparticles in flow reactors, and validated against data taken from the literature. It predicted satisfactorily the characteristics of the nanoparticles synthesized in both LFRs and SFRs, in terms of average particle size and particle size distribution standard deviation. The model points out differences of the single-phase Laminar Flow Reactor from the batch synthesis ascribable not only to direct RTD effects (with fluid elements characterized by residence times different from the average value), but also to indirect diffusion-induced effects on particle formation and growth, due to the significant mismatch in diffusivity between precursors and particles. This mismatch leads to different RTD for the two different components of the reaction mixture. In the specific case modeled in this work (the Stöber process), the indirect flow-induced effects on the synthesis can be described by *apparent* nucleation rates that change from

streamline to streamline. This work indicates that for an accurate prediction of the particle size distribution standard deviation, it is important to account for RTD effects. The model aims to make a contribution towards the development of rigorous design procedures for the continuous flow synthesis of nanoparticles, allowing more accurate optimization and control of corresponding processes.

## 6. Acknowledgments

This project has received funding from the European Union's Horizon 2020 research and innovation programme under the Marie Skłodowska-Curie grant agreement No 721290. This publication reflects only the author's view, exempting the Community from any liability.

Project website: <http://cosmic-etn.eu/>.

## References

- [1] Q. Cao, J.A. Rogers, Ultrathin films of single-walled carbon nanotubes for electronics and sensors: A review of fundamental and applied aspects, *Adv. Mater.* 21 (2009) 29–53.  
doi:10.1002/adma.200801995.
- [2] D. Jaque, L. Martínez Maestro, B. del Rosal, P. Haro-Gonzalez, A. Benayas, J.L. Plaza, E. Martín Rodríguez, J. García Solé, Nanoparticles for photothermal therapies., *Nanoscale.* 6 (2014) 9494–530.  
doi:10.1039/c4nr00708e.
- [3] M. Arruebo, R. Fernández-pacheco, M.R. Ibarra, J. Santamaría, Magnetic nanoparticles for drug delivery, *Nano Today.* 2 (2007) 22–32. doi:10.1016/S1748-0132(07)70084-1.

- [4] C. Blanco-Andujar, L.D. Tung, N.T.K. Thanh, Synthesis of nanoparticles for biomedical applications, *Annu. Reports Sect. "A" (Inorganic Chem.* 106 (2010) 553. doi:10.1039/b920666n.
- [5] P. Sharma, S. Brown, G. Walter, S. Santra, B. Moudgil, Nanoparticles for bioimaging, *Adv. Colloid Interface Sci.* 123–126 (2006) 471–485. doi:10.1016/j.cis.2006.05.026.
- [6] L. El Char, L.A. Lamont, N. El Zein, Review of photovoltaic technologies, *Renew. Sustain. Energy Rev.* 15 (2011) 2165–2175. doi:10.1016/j.rser.2011.01.004.
- [7] J. Panyam, V. Labhsetwar, Biodegradable nanoparticles for drug and gene delivery to cells and tissue, *Adv. Drug Deliv. Rev.* 55 (2003) 329–347. doi:10.1016/S0169-409X(02)00228-4.
- [8] W. Zhang, G. Frank, A. Wang, Nanoparticles in Medicine: Therapeutic Applications and Developments, *Clin. Pharmacol. Ther.* 83 (2008) 761–769. doi:10.1038/sj.clp.
- [9] S. Marre, K.F. Jensen, Synthesis of micro and nanostructures in microfluidic systems, *Chem. Soc. Rev.* 39 (2010) 1183–1202. doi:10.1039/b821324k.
- [10] B.P. Mason, K.E. Price, J.L. Steinbacher, A.R. Bogdan, D.T. Mcquade, Greener Approaches to Organic Synthesis Using Microreactor Technology, *Chem. Rev.* 107 (2007) 2300–2318. doi:10.1021/cr050944c.
- [11] A. Stankiewicz, J.A. Moulijn, Process Intensification, *Chem. Eng. Prog.* 96 (2000) 22–34. doi:10.1205/psep.04241.
- [12] Y. Xia, Y. Xiong, B. Lim, S.E. Skrabalak, Shape-controlled synthesis of metal nanocrystals: Simple chemistry meets complex physics?, *Angew. Chemie - Int. Ed.* 48 (2009) 60–103. doi:10.1002/anie.200802248.
- [13] S. Lazzari, M. Abolhasani, K.F. Jensen, Modeling of the formation kinetics and size distribution evolution of II-VI Quantum Dots, *React. Chem. Eng.* (2017). doi:10.1039/C7RE00068E.
- [14] J.Y. Rempel, M.G. Bawendi, K.F. Jensen, Insights into the kinetics of semiconductor nanocrystal

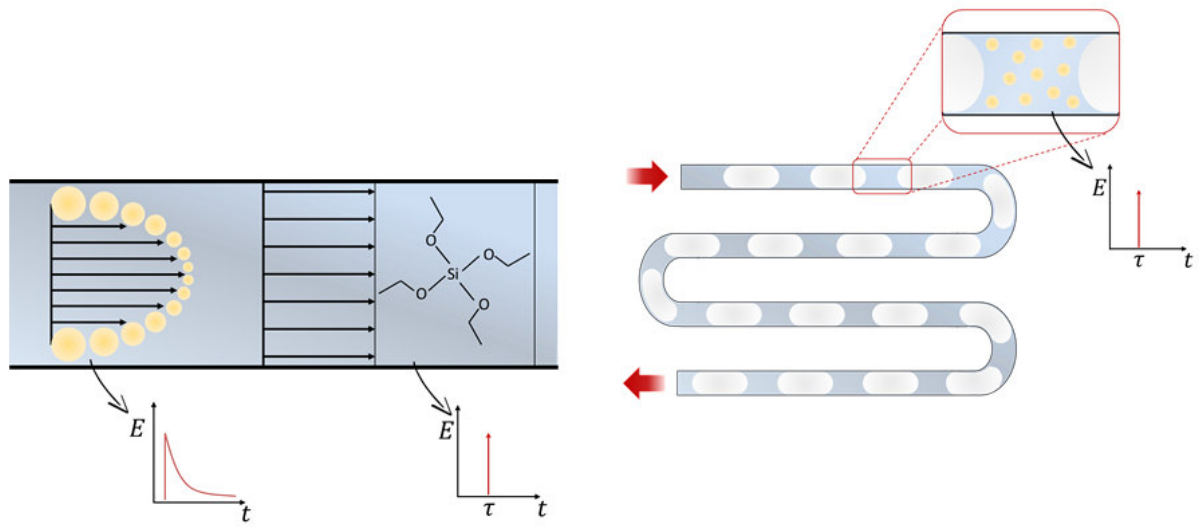
- nucleation and growth, *J. Am. Chem. Soc.* 131 (2009) 4479–4489. doi:10.1021/ja809156t.
- [15] P. Stolzenburg, G. Garnweitner, Experimental and numerical insights into the formation of zirconia nanoparticles: A population balance model for the nonaqueous synthesis, *React. Chem. Eng.* 2 (2017) 337–348. doi:10.1039/C7RE00005G.
- [16] R.M. Maceiczky, L. Bezing, A.J. deMello, Kinetics of nanocrystal synthesis in a microfluidic reactor: theory and experiment, *React. Chem. Eng.* 1 (2016) 261–271. doi:10.1039/C6RE00073H.
- [17] O. Levenspiel, *Chemical Reaction Engineering*, John Wiley & Sons, 1962. doi:10.1016/0009-2509(64)85017-X.
- [18] T.M. Squires, S.R. Quake, Microfluidics: Fluid physics at the nanoliter scale, *Rev. Mod. Phys.* 77 (2005) 977–1026. doi:10.1103/RevModPhys.77.977.
- [19] S.A. Khan, A. Günther, M.A. Schmidt, K.F. Jensen, Microfluidic synthesis of colloidal silica, *Langmuir*. 20 (2004) 8604–8611. doi:10.1021/la0499012.
- [20] A. Günther, S.A. Khan, M. Thalmann, F. Trachsel, K.F. Jensen, Transport and reaction in microscale segmented gas-liquid flow., *Lab Chip*. 4 (2004) 278–286. doi:10.1039/b403982c.
- [21] S. Krishnadasan, J. Tovilla, R. Vilar, a. J. deMello, J.C. deMello, On-line analysis of CdSe nanoparticle formation in a continuous flow chip-based microreactor, *J. Mater. Chem.* 14 (2004) 2655. doi:10.1039/b401559b.
- [22] L. Gutierrez, L. Gomez, S. Irusta, M. Arruebo, J. Santamaria, Comparative study of the synthesis of silica nanoparticles in micromixer-microreactor and batch reactor systems, *Chem. Eng. J.* 171 (2011) 674–683. doi:10.1016/j.cej.2011.05.019.
- [23] S.E. Lohse, J.R. Eller, S.T. Sivapalan, M.R. Plews, C.J. Murphy, A Simple Millifluidic Benchtop Reactor System for the High-Throughput Synthesis and Functionalization of Gold Nanoparticles with Different Sizes and Shapes, *ACS Nano*. 7 (2013) 4135–4150. doi:10.1021/nn4005022.

- [24] W.R. Dean, The stream-line motion of fluid in a curved pipe, London, Edinburgh, Dublin Philos. Mag. J. Sci. 5 (1928) 673–695.
- [25] V. Ananthkrishnan, W.N. Gill, A.J. Barduhn, Laminar dispersion in capillaries: Part I. Mathematical analysis, *AIChE J.* 11 (1965) 1063–1072. doi:10.1002/aic.690110620.
- [26] G.I. Taylor, Dispersion of soluble matter in solvent flowing slowly through a tube, *Proc. R. Soc. A Math. Phys. Eng. Sci.* 223 (1954) 446–468. doi:10.1098/rspa.1983.0054.
- [27] R. Aris, On the dispersion of a solute in pulsating flow through a tube, *Proc. R. Soc. A Math. Phys. Eng. Sci.* 259 (1960) 370–376. doi:10.1098/rspa.1983.0054.
- [28] D. Rossi, L. Gargiulo, G. Valitov, A. Gavriilidis, L. Mazzei, Experimental characterization of axial dispersion in coiled flow inverters, *Chem. Eng. Res. Des.* 120 (2017) 159–170. doi:10.1016/j.cherd.2017.02.011.
- [29] F. Trachsel, A. Günther, S. Khan, K.F. Jensen, Measurement of residence time distribution in microfluidic systems, *Chem. Eng. Sci.* 60 (2005) 5729–5737. doi:10.1016/j.ces.2005.04.039.
- [30] B.L. Cushing, V.L. Kolesnichenko, C.J. O'Connor, Recent advances in the liquid-phase syntheses of inorganic nanoparticles, *Chem. Rev.* 104 (2004) 3893–3946. doi:10.1021/cr030027b.
- [31] J. Polte, Fundamental Growth Principles of Colloidal Metal Nanoparticles - a new Perspective, *CrystEngComm.* 17 (2015) 6809–6830. doi:10.1039/C5CE01014D.
- [32] J. Park, J. Joo, G.K. Soon, Y. Jang, T. Hyeon, Synthesis of monodisperse spherical nanocrystals, *Angew. Chemie - Int. Ed.* 46 (2007) 4630–4660. doi:10.1002/anie.200603148.
- [33] V.S. Cabeza, S. Kuhn, A. a Kulkarni, K.F. Jensen, Size-Controlled Flow Synthesis of Gold Nanoparticles Using a Segmented Flow Micro fluidic Platform, 30th Anniv. *Langmuir.* 28 (2012) 7007–7013. doi:10.1021/la205131e.
- [34] M.J.F. Warnier, E. V. Rebrov, M.H.J.M. de Croon, V. Hessel, J.C. Schouten, Gas hold-up and liquid film

- thickness in Taylor flow in rectangular microchannels, *Chem. Eng. J.* 135 (2007) 153–158.  
doi:10.1016/j.cej.2007.07.008.
- [35] A.A. Kulkarni, V.S. Kalyani, Two-phase flow in minichannels: Hydrodynamics, pressure drop, and residence time distribution, *Ind. Eng. Chem. Res.* 48 (2009) 8193–8204. doi:10.1021/ie801937x.
- [36] L. Yang, M.J. Nieves-Remacha, K.F. Jensen, Simulations and analysis of multiphase transport and reaction in segmented flow microreactors, *Chem. Eng. Sci.* 169 (2017) 106–116.  
doi:10.1016/j.ces.2016.12.003.
- [37] W. Salman, P. Angeli, A. Gavriilidis, Sample pulse broadening in Taylor flow microchannels for screening applications, *Chem. Eng. Technol.* 28 (2005) 509–514. doi:10.1002/ceat.200500008.
- [38] G.H. Bogush, C.F. Zukoski IV, Studies of the kinetics of the precipitation of uniform silica particles through the hydrolysis and condensation of silicon alkoxides, *J. Colloid Interface Sci.* 142 (1991) 1–18. doi:10.1016/0021-9797(91)90029-8.
- [39] G.H. Bogush, C.F. Zukoski IV, Uniform silica particle precipitation: An aggregative growth model, *J. Colloid Interface Sci.* 142 (1991) 19–34. doi:10.1016/0021-9797(91)90030-C.
- [40] G.H. Bogush, M.A. Tracy, C.F. Zukoski IV, Preparation of monodisperse silica particles: Control of size and mass fraction, *J. Non. Cryst. Solids.* 104 (1988) 95–106. doi:10.1016/0022-3093(88)90187-1.
- [41] T. Matsoukas, E. Gulari, Dynamics of growth of silica particles from ammonia-catalyzed hydrolysis of tetra-ethyl-orthosilicate, *J. Colloid Interface Sci.* 124 (1988) 252–261. doi:10.1016/0021-9797(88)90346-3.
- [42] T. Matsoukas, E. Gulari, Monomer-addition growth with a slow initiation step: A growth model for silica particles from alkoxides, *J. Colloid Interface Sci.* 132 (1989) 13–21. doi:10.1016/0021-9797(89)90210-5.
- [43] A. Van Blaaderen, J. Van Geest, A. Vrij, Monodisperse colloidal silica spheres from tetraalkoxysilanes: Particle formation and growth mechanism, *J. Colloid Interface Sci.* 154 (1992) 481–501.

- doi:10.1016/0021-9797(92)90163-G.
- [44] D.L. Green, J.S. Lin, Y.F. Lam, M.Z.C. Hu, D.W. Schaefer, M.T. Harris, Size, volume fraction, and nucleation of Stober silica nanoparticles, *J. Colloid Interface Sci.* 266 (2003) 346–358.  
doi:10.1016/S0021-9797(03)00610-6.
- [45] D.L. Green, S. Jayasundara, Y.F. Lam, M.T. Harris, Chemical reaction kinetics leading to the first Stober silica nanoparticles - NMR and SAXS investigation, *J. Non. Cryst. Solids.* 315 (2003) 166–179.  
doi:10.1016/S0022-3093(02)01577-6.
- [46] V.K. LaMer, R.H. Dinegar, Theory, Production and Mechanism of Formation of Monodispersed Hydrosols, *J. Am. Chem. Soc.* 72 (1950) 4847–4854. doi:10.1021/ja01167a001.
- [47] K. Lee, A.N. Sathyagal, A. V. McCormick, A closer look at an aggregation model of the Stöber process, *Colloids Surfaces A Physicochem. Eng. Asp.* 144 (1998) 115–125. doi:10.1016/S0927-7757(98)00566-4.
- [48] D. Nagao, T. Satoh, M. Konno, A Generalized Model for Describing Particle Formation in the Synthesis of Monodisperse Oxide Particles Based on the Hydrolysis and Condensation of Tetraethyl Orthosilicate, *J. Colloid Interface Sci.* 232 (2000) 102–110. doi:10.1006/jcis.2000.7195.
- [49] E.J.W. Verwey, J.T.G. Overbeek, Theory of the stability of lyophobic colloids, 1947.
- [50] H. Reerink, J.T.G. Overbeek, The rate of coagulation as a measure of the stability of silver iodide sols, *Discuss. Faraday Soc.* 18 (1954) 74. doi:10.1039/df9541800074.
- [51] S. Kim, C.F. Zukoski, A model of growth by hetero-coagulation in seeded colloidal dispersions, *J. Colloid Interface Sci.* 139 (1990) 198–212. doi:10.1016/0021-9797(90)90457-Y.
- [52] L.A. Wijenayaka, M.R. Ivanov, C.M. Cheatum, A.J. Haes, Improved parametrization for extended derjaguin, landau, verwey, and overbeek predictions of functionalized gold nanosphere stability, *J. Phys. Chem. C.* 119 (2015) 10064–10075. doi:10.1021/acs.jpcc.5b00483.

- [53] J. Aubin, L. Prat, C. Xuereb, C. Gourdon, Effect of microchannel aspect ratio on residence time distributions and the axial dispersion coefficient, *Chem. Eng. Process. Process Intensif.* 48 (2009) 554–559. doi:10.1016/j.cep.2008.08.004.
- [54] M. Wörner, Approximate residence time distribution of fully develop laminar flow in a straight rectangular channel, *Chem. Eng. Sci.* 65 (2010) 3499–3507. doi:10.1016/j.ces.2010.02.047.
- [55] M. Abolhasani, C.W. Coley, L. Xie, O. Chen, M.G. Bawendi, K.F. Jensen, Oscillatory Microprocessor for Growth and in Situ Characterization of Semiconductor Nanocrystals, *Chem. Mater.* 27 (2015) 6131–6138. doi:10.1021/acs.chemmater.5b02821.
- [56] A.M. Nightingale, J.C. de Mello, Microscale synthesis of quantum dots, *J. Mater. Chem.* 20 (2010) 8454. doi:10.1039/c0jm01221a.



ACCEPTED MANUSCRIPT

**Highlights**

- A model for the design of microreactors synthesising nanoparticles is proposed;
- The model utilises only kinetics and diffusion parameters from the literature;
- Residence time distribution effects on nanoparticle size distribution is quantified;
- Effects of transport phenomena on reaction kinetics in the flow synthesis are shown.

ACCEPTED MANUSCRIPT